Journal of Thermal Science Vol.30, No.5 (2021) 1596–1606

https://doi.org/10.1007/s11630-021-1438-z **Article ID: 1003-2169(2021)05-1596-11**

Numerical and Experimental Investigation on Heat Transfer Performance of a Solar Single Storage Tank

MAO Qianjun, LI Ying, ZHANG Yamei, ZHANG Chunzhi*

School of Urban Construction, Wuhan University of Science and Technology, Wuhan 430065, China

Abstract: The single-tank latent heat thermal energy storage (LHTES) of solar energy mainly consists of two modules: the first one is the phase change material (PCM) module heated by solar energy; the second is a module of heat transfer between melted PCM and the user's low-temperature water. This paper mainly focuses on the former one. To investigate the heat transfer performance of the paraffin-based solar single storage tank and find a more suitable experimental configuration, as basic research work, we established a single-tank thermal storage platform and then conducted a numerical simulation on the heat transfer process with Fluent. The result of numerical simulation shows that the test situation was basically reflected and the data agreed well with the experiment results. The numerical simulation analysis is accurate and the method is reliable. To obtain the heat transfer performance of paraffin in a single tank and strengthen heat transfer, the aspect ratio, the melting temperature of paraffin, and the heating power of the electric heater were analyzed based on simulation. The results show that the heat transfer gets more uniform when the aspect ratio is lower. This results in an increase in the liquid fraction of 61.83% to 76.47% one hour after heating when the aspect ratio of the tank reduced from 2.8 to 1.1. The higher the melting temperature of paraffin, the longer it takes for PCM to reach a stable state. And the curvature of liquid heating is greater than that of solid heating at the bottom layer. Under the constant total work, the heating power has little effect on the heat transfer performance of the paraffin. This study will provide some reference value for the optimization design of single-tank LHTES systems in the future.

Keywords: LHTES, single tank, PCM, numerical simulation

1. Introduction

Nowadays, energy shortage and environmental pollution have gradually become bottlenecks restricting China's social and economic development. On the general trend of the development of renewable energy, solar energy has gradually shown its advantages, and many scholars have conducted in-depth research on solar energy thermal storage [1–3], such as electric heat storage [4] and energy collection [5].

At present, LHTES is at a stage of rapid development, which is of great significance in solar energy utilization [6, 7]. Meanwhile, the development of heat storage in double tank molten salt is relatively mature. However, for the double storage tank, the volume of nearly one tank is not fully utilized, and the cost of the double tanks is relatively high, which makes the technology of heat storage in a single tank to come to be valued. The solar

Received: Oct 12, 2019 AE: LI Yinshi Corresponding author: ZHANG Chunzhi E-mail: zhangchunzhi@wust.edu.cn
Special Column: Advancement in Solar Energy Technologies

Nomenclature

A	mushy zone constant, $A=1\times10^{-5}$ kg·m^{-3}·s^{-1}	Y	kinematic viscosity/m^2·s^{-1}
C_p	specific heat/J·kg^{-1}·K^{-1}	**Greek symbols**	
H	total enthalpy/J·kg^{-1}	β	volumetric expansion coefficient/K^{-1}
h	enthalpy/J·kg^{-1}	ε	numerical constant
k	thermal conductivity/W·m^{-1}·K^{-1}	μ	dynamic viscosity/kg·m^{-1}·s^{-1}
L	latent heat/J·kg^{-1}	ρ	density/kg·m^{-3}
m	mass of PCM/kg	**Subscripts**	
P	pressure/Pa	L	melting point
q_v	source term/W·m^{-3}	mush	mushy zone
T	temperature/K	o	reference
t	time/s	S	solidification point
v	velocity/m·s^{-1}		

single storage tank is mainly used in two configurations: the packed bed storage tank and the tube-in-shell cylindrical storage tank.

For the packed bed storage tank, Xu et al. [8–10] analyzed the two-dimensional distribution of temperature, the development of the oblique temperature layer in the storage and exothermic process of a single tank packed bed heat storage system based on the two-phase model. Wu et al. [11] studied the transient heat release behavior and characteristics under different conditions of a phase-change packed bed with a temperature range of 563 K to 663 K based on the mixed diffusion model. Bellan [12–14], Kodama [15], and Miguel et al. [16] established the bed model and analyzed the heat transfer characteristics between the PCM microcapsules in the heat storage system and the heat transfer fluid.

For the tube-in-shell cylindrical storage tank, Tay et al. [17] established a new spiral heat exchanger tube-in-shell heat transfer system. The stability and duration of the system were investigated by experiments and CFD modeling. Seddegh et al. [18–20] researched vertical and horizontal cylindrical tube-in-shell LHTES and carried out visualization experiments. The influence of natural convection on the heat transfer of PCM was considered. Mao et al. [21–23] established a new three-dimensional heat transfer model and optimized a novel duct-shell TES tank. Joybari et al. [24] proposed a leading-edge tracking method for the melting interface under the influence of natural convection, and then conducted an in-depth study on the phase change heat transfer process in the horizontal tube-in-shell heat exchanger. Justin et al. [25–27] explored the enhanced heat transfer and energy storage design of the tube-in-shell phase change heat storage system considering the effect of natural convection.

The above researches show that high-temperature molten salt is widely used in the field of heat storage in the packed bed storage tank, and many calculation models are derived based on it. In the field of tube-in-shell cylindrical storage tanks, natural convection and tank structure have a great influence on the rate of heat storage. Although much work has focused on single tank heat storage systems so far, most of the studies concentrate on high-temperature molten salt and few studies on low-temperature PCM (phase change temperature ≤373 K). The molten salt pump is used in the single tank heat storage system with ordinary molten salt, which is complicated and easy to be corroded [28]. High-temperature molten salt and air contact will cause oxidation degradation, so the heat exchange system shall be required for sealing. It is easy to form a high-temperature and high-pressure environment and generate hazards during the process [29]. Moreover, the heat storage of molten salt will gradually degrade in a long cycle, and the technology of enhancing heat transfer of molten salt is complex and relatively expensive [30, 31]. Among all available solar PCMs, paraffin owns the advantages of being non-toxic, relatively inexpensive, compatible with metal sheathing [32] and stable in the long term [33]. In this paper, the PCM module in a typical solar energy phase change storage system is analyzed. Due to the instability of solar radiation, electric heating is used in place of solar energy. The purpose of this paper is to evaluate the heat transfer performance of a single solar energy storage tank filled with low-temperature paraffin wax. Aiming to improve the performance of this system, experiments are carried out at room temperature of 300 K. The influences of the aspect ratio of the tank, melting temperature of paraffin, and heater power on the heat transfer process are analyzed through Fluent numerical simulation.

2. Models and Verification

2.1 Physical model

In the experimental setup mentioned in this paper, the low-temperature PCM, high-efficiency chip paraffin, is

used as a heat storage medium. The tank body is made of austenitic stainless steel (SUS316L) [34]. To ensure the accuracy of the experimental results, adiabatic boundary conditions are guaranteed as far as possible. The shell of the tank body is surrounded by insulation material Q235B aluminosilicate cotton with a thickness of 200 mm.

In the calculation, a cylindrical storage tank is selected as the physical model, with a diameter of 230 mm and a height of 350 mm. For ensuring the safety of tank, a 10 mm deep arc groove was left at the bottom, regardless of the thickness of the tank wall. The U type unilateral length of the heating tube of the selected electric heater is 330 mm, all of which are arranged in an annular cross array. The wall thickness of the heating tube is 1.5 mm; the flange size is DN150, and the length of the heat dissipation section is designed to be 150 mm. There is a 50 mm non-heating zone at the upper connecting junction box of the heater. The bottom of the heating tube is 20 mm from the bottom of the cylinder part of the tank. The tank is filled with 12 kg paraffin and 2 kg paraffin in the groove at the bottom is removed. The actual paraffin involved in the reaction is about 10 kg. For the sake of eliminating the expansion of paraffin during melting, the filling degree of paraffin in the tank is not 100%.

During the numerical simulation, the heat transfer model of the paraffin-based tank is obtained by simplifying the system, as shown in Fig. 1. All measuring points are arranged at a horizontal distance of 120 mm from the center of gravity of the tank. The top measuring points 1 and 2 are located at a vertical distance of 200 mm from the bottom of the tank; the middle measuring points 3 and 4, and the bottom measuring points 5 and 6 are 100 mm and 0 mm, respectively [34].

At the beginning of the melting process, the coupling layer of paraffin and heater surface begins to melt, then the natural convection is generated by the temperature difference and the heat transfer process is speeded. The heat transfer performance of PCM inside the tank is in the form of an irregular diffusion movement.

2.2 Mathematical model

In order to ensure the accuracy of the model as much as possible and save the calculation time, only the heat transfer behavior in the heating tube area and the PCM area in the tank was studied, and the simulation calculation model was obtained by appropriately simplifying the experimental process. The assumptions about the mathematical model are as follows:

(1) The PCM area in the tank is a continuous and homogeneous porous media area (excluding the middle heating tube area). The physical properties of PCM are independent of temperature and the homogenization is isotropic [35, 36];

(2) The axial and radial heat transfer inside the heating tube is neglected;

(3) The adiabatic wall is assumed;

(4) The heat conduction and radiation heat transfer between the PCM area of single tank heat storage and the tank body is ignored, and radiation heat transfer between heated paraffin and unheated paraffin is ignored too;

(5) Ignoring the influence of heat transfer thermal resistance;

(6) The PCM is incompressible after melting. The Boussinesq approximation is adopted to consider natural convection in the phase change area [37].

An equilibrium equation was established according to the coupling heat transfer relationship. The paraffin in the tank is heated by a heater with a constant power of 3 kW for 12 min through an internal body heat source in the PCM area, based on the consideration that the total work of a constant power of 3 kW heating for the 12 min equals to the latent heat of all the paraffin in the tank.

The governing equations are listed as follows:

$$\rho C_p \frac{\partial T}{\partial t} = \frac{\partial}{\partial x}\left(k\frac{\partial T}{\partial x}\right) + \frac{\partial}{\partial y}\left(k\frac{\partial T}{\partial y}\right) + \frac{\partial}{\partial z}\left(k\frac{\partial T}{\partial z}\right) + q_v \tag{1}$$

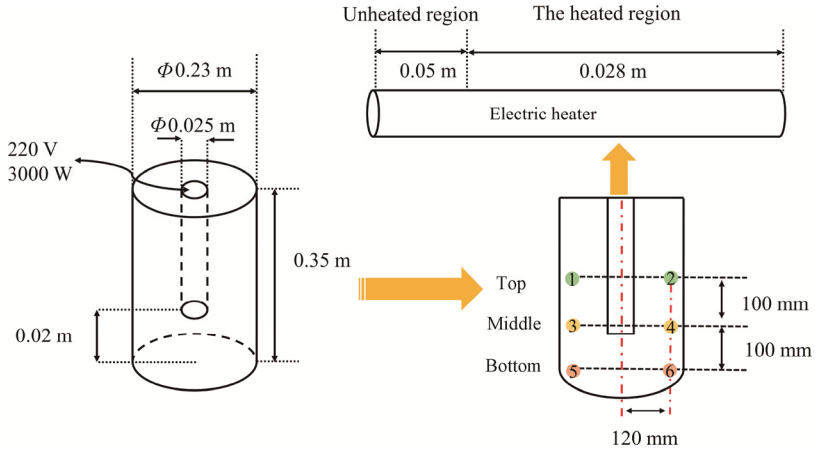

Fig. 1 Schematic diagram of electric heating paraffin-based single tank heat storage system

$$q_v = \frac{W}{V_{\text{Heat}}} \tag{2}$$

$$Wt_{\text{Heat}} = mL \tag{3}$$

where W is the power of the heater; V_{heat} is the volume of the heating tube; t_{Heat} is the time for heating.

Since the phase change problem is a nonlinear transient heat transfer problem, enthalpy is used as a variable function to solve the interface tracking of the phase change problem by substituting it into the heat transfer differential equation to solve the temperature field [38, 39]. The enthalpy model is used to deal with the flow boundary problem in the process of solid-liquid change. The corresponding governing equation is given as follows [21]:

$$\frac{\partial \rho H}{\partial t} + \nabla(\rho v H) = \nabla(k \cdot \Delta T) + q_v \tag{4}$$

In this paper, the enthalpy function is defined as the sum of sensible heat capacity and latent heat of phase change. It is a temperature-related function, and its specific expression is as follows [20]:

$$H = h + fL \tag{5}$$

$$h = h_0 + \int_{T_0}^{T} C_p \mathrm{d}T \tag{6}$$

where h_0 is the sensible enthalpy of PCM when the temperature is T_0. According to Eq. (7), f is the liquid fraction of paraffin, which indicates the proportion of the liquid volume in the calculated region to the total volume.

$$f = \begin{cases} 0 & T < T_{\text{S}} \\ \dfrac{T - T_{\text{S}}}{T_{\text{L}} - T_{\text{S}}} & T_{\text{S}} \le T \le T_{\text{L}} \\ 1 & T > T_{\text{L}} \end{cases} \tag{7}$$

The simplified energy equation is shown as follows:

$$\frac{\partial \rho H}{\partial t} + \nabla(\rho v h) = \nabla(k \cdot \Delta T) - \frac{\partial \rho f L}{\partial t} - \nabla(\rho v f L) + q_v \tag{8}$$

The momentum equation above is based on the Boussinesq hypothesis. It is assumed that the density of paraffin is constant in all equations, but the force term is not taken into account, where it is modeled based on the reference density (ρ_0), temperature (T_0) and volume expansion coefficient (β).

Momentum equation:

$$\frac{\partial \rho_0 h}{\partial t} + \nabla(\rho_0 v v) = -\nabla P + \nabla(\mu \nabla v) + (\rho - \rho_0) g + \frac{(1-f)^2}{f^3 + \varepsilon} v A_{\text{mush}} \tag{9}$$

Boussinesq hypothesis:

$$(\rho - \rho_0) g = -\rho_0 \beta (T - T_0) \tag{10}$$

Continuity equation:

$$\frac{\partial \rho}{\partial t} + \nabla(\rho \cdot v) = 0 \tag{11}$$

After heating, there is no internal heat source in the PCM area, and internal heat transfer is only generated by natural convection caused by temperature difference. According to Eq. (1), the governing equation can be expressed as:

$$\rho c \frac{\partial T}{\partial t} = \frac{\partial}{\partial x}\left(k \frac{\partial T}{\partial x}\right) + \frac{\partial}{\partial y}\left(k \frac{\partial T}{\partial y}\right) + \frac{\partial}{\partial z}\left(k \frac{\partial T}{\partial z}\right) \tag{12}$$

Materials used in the simulation include paraffin and steel. According to the data provided by the corresponding manufacturer, the physical parameters of the materials are shown in Table 1.

Table 1 Values of the relevant material properties used in the simulation

Physical quantity	Value
Paraffin wax	
Density	850 kg·m^{-3}
Thermal conductivity	0.2 W·m^{-1}·K^{-1}
Specific heat capacity	2000 J·kg^{-1}·K^{-1}
Latent heat of fusion	140 kJ·kg^{-1}
Melting initial temperature	321 K
Melting final temperature	323 K
Dynamic viscosity	1.72×10^{-5} kg·m^{-1}·s^{-1}
Thermal expansion coefficient	0.0006 K^{-1}
Steel	
Density	8030 kg·m^{-3}
Thermal conductivity	16.27 W·m^{-1}·K^{-1}
Specific heat capacity	502.48 J·kg^{-1}·K^{-1}

2.3 Experimental setup

The experimental platform is built, and the whole set of equipment is designed. Fig. 2 is a picture of the small-scale test facility.

In the design process of the solar energy single-tank heat storage system, the material of the heat storage tank should conform to the temperature variation range of the heat storage medium and meet its highest working temperature. Also, attention should be paid to the chemical compatibility between the heat storage medium and the heat storage tank material. The long-term paraffin melting and solidification process will lead to the reaction between the electric heating layer and heat storage tank surface and the formation of the oxide film, thus affecting the actual heating power of the heater and the overall experimental results. Therefore, with the above consideration, the electric heater uses a SUS310S seamless steel tube, and the water tank uses SUS316L austenitic stainless steel.

Table 2 presents the specific parameters for the main equipment. The introduction of the main instruments is as follows:

Table 2 Main parameters of the experimental measuring instruments

Parameter	Instrument	Instrument model	Range	Accuracy
Temperature	Thermocouple	SYWRNK-191/K	3 K to 2588 K	0.1 K
Temperature	Data Acquisition Unit	Fluke 2638A	3 K to 673 K	0.08 K
Distribution of temperature	Infrared thermography	Fluke Ti-32	253 K to 873 K	2 K/2%

(1) Data acquisition instrument: FLUKE 2638A HYDRA Series III data acquisition unit is used for data recording, which cooperates with the FLUKE DAQ 4.0 software as a data acquisition system. The data acquisition instrument has 3 layers and 22 connection channels, and the data recording interval can be adjusted. For the K-type thermocouple, the sampling rate can reach 0.01 K/s at a temperature of 300 K.

(2) Heat storage tank: The main material is SUS316L austenitic stainless steel, and the shell of the tank is made of Q235B aluminum silicate cotton with a thickness of 200 mm. The tank capacity is 0.0185 m^3.

(3) High-temperature armored thermocouple: Six high-temperature armored thermocouples are connected to the data recorder at the measuring point inside the paraffin body of the tank. The thermocouple is made of SYWRNK-191K thermocouple with cold end compensation joint and probe rod with a diameter of 3–4 mm and is equipped with a temperature compensation lead which is resistant to high temperature and interference.

(4) Flange electric heater: The experiment adopts the flange heating tube with the power of 3 kW and the heating temperature up to 823 K. The SUS310S seamless steel tube and the Cr20Ni80 nickel-chromium alloy are adopted. The distribution is a uniform annular cross inside the heater. The inner and outer diameters of the flange are 285 mm and 240 mm respectively. The diameter of the small hole is 22 mm. The 8 small holes are evenly distributed on the same circumference, which is used for placing thermocouples and preventing the production of high temperature and high-pressure environment to ensure the safety of the experiment.

(5) Infrared thermography: The temperature measurement range of FLUKE Ti32 IR fusion infrared thermography is 253 K to 873 K. The accuracy is ±2 K/2%, and the thermal sensitivity is no more than 0.05 K. The experiment is used to observe the temperature distribution of the phase-change material in the tank to determine how it melted.

After 9 cycles of melting and solidification, the thermophysical properties of paraffin did not change [31]. Then the formal experiments and data records are conducted after the thermocouple being arranged and fixed. The digital recorder is preheated for half an hour. The paraffin is heated for 12 min at a fixed power of 3 kW and then the power is turned off. Data are recorded with a recording interval of 5 s during heating and 5 min during standing melting. Finally, data are imported into the computer in the format of the CSV data table for analysis.

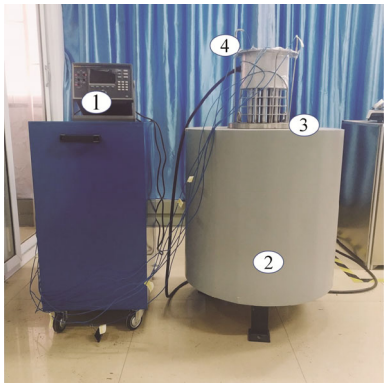

Fig. 2 Picture of the small-scale test facility: (1) data acquisition unit, (2) tank, (3) electric flange heater and (4) thermocouple

2.4 Calculation and verification

Since there is radial heat transfer after heating and the influence of gravity cannot be ignored, the tank and flange heater are both three-dimensionally symmetrical, and the internal pressure and temperature distribution are symmetrical. In order to balance the calculation resources, it is more reasonable to take 1/4 of the circular section of the tank, flange heater and the three-dimensional space of the length direction as the calculation area.

The 3D numerical simulation is carried out by FLUENT 16.0. The non-structured hexahedral mesh is used to discrete the computation domain. The PRESTO! scheme is employed for pressure correction, and the SIMPLE algorithms are adopted for pressure and velocity coupling. The Green-Gauss Node Based is used for the spatial discretization of the gradient. The rest of the settings and relaxation factors are left by default.

Interval sizes 5, 2.5, 2, and 1 are selected respectively, with corresponding grid numbers of 8448, 67 584, 134 200, and 1 056 000. The four grid forms are used to calculate the temperature field. The phase change process durations under the four different grids are nearly the same, 780 min. The larger the number of grids, the longer the actual computing time. The actual computing time corresponding to the four grids is 1179 minutes, 1519 minutes, 1643 minutes, and 2165 minutes respectively.

Therefore, the number of grids 8448 is chose, which is enough to obtain accurate results, and the computation time is the shortest. After the optimal combination calculation of the time step and the maximum number of iterations, the time step is 1 s, and the maximum number of iterations is 20.

To verify the reliability of the above model and the calculated results, the simulation results are compared with the experimental results. The experimental data of June 11, 2019, are selected. It is cloudy and the indoor temperature is 300 K. All the time points in the following figures start from the end of 12-min heating, i.e., the 0 min in the figures corresponds to the end of heating, which means that the power is off and heat transfer inside paraffin begins.

Fig. 3 illustrates the simulated liquid fraction variance with time during the melting process. In combination with Fig. 5, the paraffin wax on the upper layer melt rapidly after the 12-min heating, and the liquid fraction reached 38.7%. Within 1 h after heating, the liquid fraction of paraffin increased rapidly, reaching 75.55% at the 60 min. Within 1–13 h, the rising trend of paraffin liquid fraction gradually slowed down, and the curvature gradually decreased. Finally, it reached a stable value and close to 98.95% of 100%. The dead zone near the bottom of the tank was 1.05%.

In Fig. 4, the top, middle, and bottom represent the average temperature of measuring points in this layer. The maximal temperature difference between the two measuring points for the bottom layer, the middle layer, and the top layer is 0.52 K, 0.8 K and 1.02 K, respectively.

Fig. 4 shows the comparison between the experimental results and the numerical simulation results [40], which show that the two are in good agreement. The figure shows that the temperature curves of measuring points obtained in the experiment are generally below the simulation curves, and the system has a certain degree of heat loss on the whole. Moreover, the experiment lasted for a long time, and the indoor temperature fluctuated to a certain extent, which had a slight impact on the experimental results. The upper layer of paraffin has a certain amount of heat exchange with the outside through the upper part of the tank, resulting in the largest

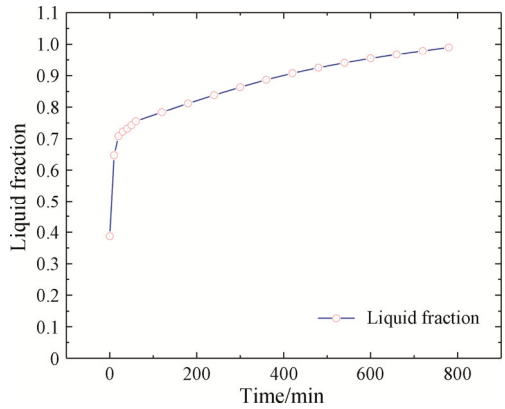

Fig. 3 Simulated liquid fraction variance with time during the melting process

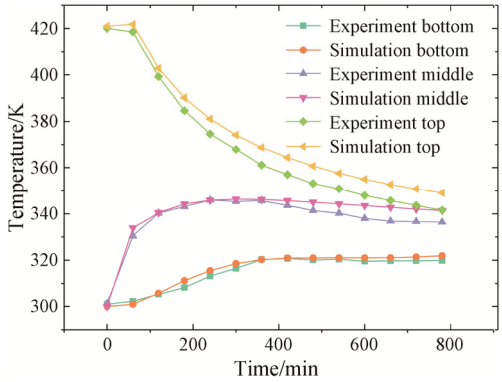

Fig. 4 Comparison between the present numerical simulation and experimental data of temperature profile in the melting process [40]

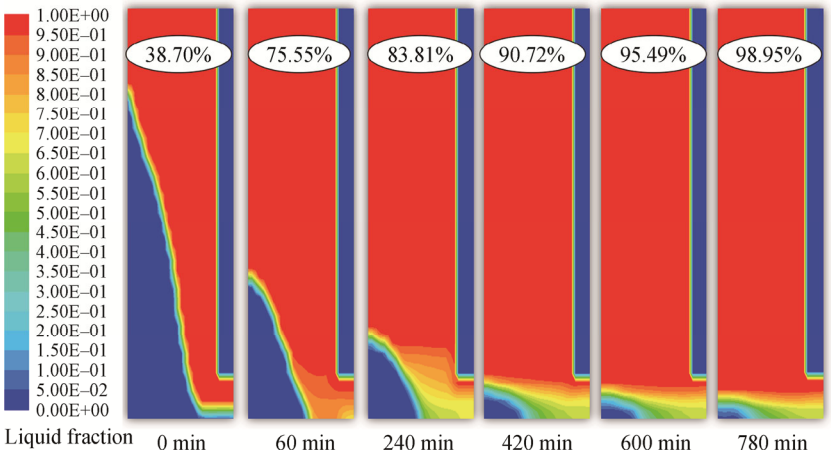

Fig. 5 Simulated liquid fraction profiles in the melting process

deviation of the upper measurement point. The average relative errors between the experimental and simulation results of the bottom, middle and upper measuring points are 2.11%, 3.83% and 7.07%, respectively. It can be seen that the calculation results of this model are in good agreement with the experimental data, that is to say, the numerical prediction and analysis based on this model are reasonable. Because of the instantaneity of the heat storage process, both static system error and dynamic system error exists in the temperature measurement system. Also, since the thermocouple is fixed at a place 120 mm away from the tank axis, the measuring point of the thermocouple may be offset to some extent in the process of paraffin melting, so there may be some errors between the experimental data and the real situation. The simulation calculation of Fluent is relatively large compared with the experimental data, which may be related to the selection of characteristic temperature in the process of coefficient solving and needs to be further studied.

3. Results and Discussion

In this section, the effects of the aspect ratio of the tank, the melting temperature of the paraffin, and the heating power of the electric heater on the heat transfer characteristics of paraffin inside the tank were explored by the numerical model. The initial temperature is 300 K for all calculations.

3.1 Effects of the aspect ratio of tank

For investigating the effects of the aspect ratio of the tank on the heat transfer performance of a single paraffin-based tank, we try to ensure a certain volume of the tank. The degree of paraffin filling and the volume of the heating tube remain unchanged. 5 groups of different combinations of height and diameter are selected. The specific combinations of height and diameter are shown in Table 3.

Fig. 6 shows the melting curves of PCM in tanks with different aspect ratios. Combined with Fig. 7 and Fig. 8, at the end of heating, the melted paraffin content in Cylinder B is the highest, and at 1 h after the end of heating, the melted paraffin content in Cylinder E is the highest. From the graph, the melting curves reach a turning point almost at the same time. The corresponding value of Cylinder E is the largest. On the whole, the smaller the aspect ratio is, the stronger the natural convection effect is and the shorter the melting time is required. When the aspect ratio is closer to 1, the temperature field in the tank is more uniform and the melting is faster. This is due to the fact that the radial and

Table 3 Specifications of the investigated cylinder tank systems

LHTES unit	Height/mm	Radius/mm	Height /Radius ratio	Mass of paraffin/kg
Cylinder A	310	110	2.8	10.01
Cylinder B	260	120	2.2	9.99
Cylinder C	220	130	1.7	9.92
Cylinder D	190	140	1.4	9.94
Cylinder E	165	150	1.1	9.91

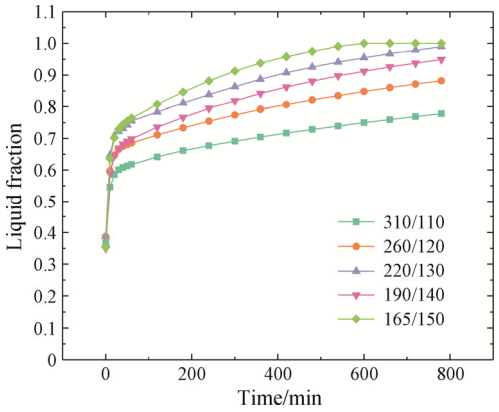

Fig. 6 The liquid fraction with different aspect ratio

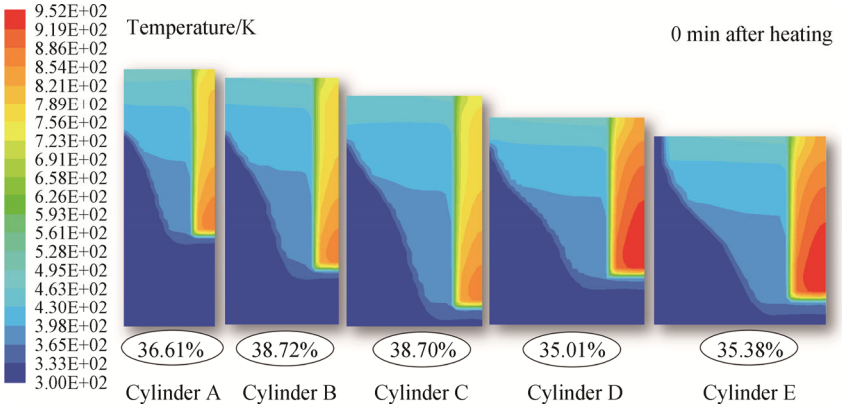

Fig. 7 Temperatures profiles at 0 min after heating

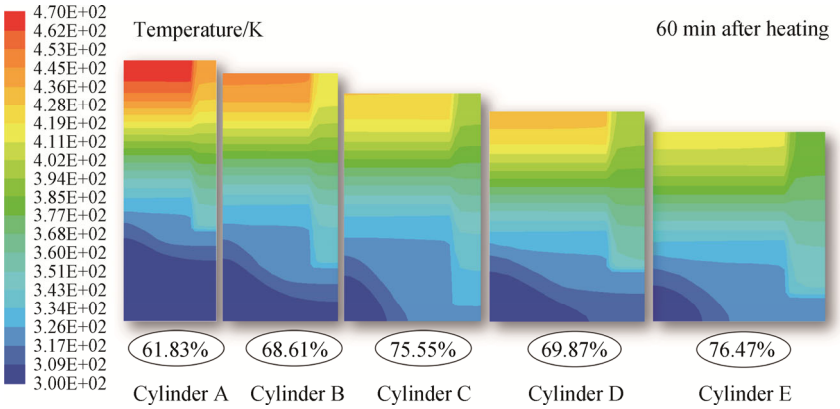

Fig. 8 Temperatures profiles at 60 min after heating

axial diffusion of natural convection are almost completed at the same time. This caused the liquid fraction to increase from 61.83% to 76.47% 1 h after heating when the aspect ratio of the tank decreases from 2.8 to 1.1.

3.2 Effects of melting temperature of paraffin

To investigate the effects of different paraffin melting temperature on heat transfer characteristics of the paraffin-based single tank, 10 K is taken as a gradient, and other properties are unchanged. The melting temperatures of paraffin were selected as 351–353 K, 341–343 K, 331–333 K, and 311–313 K, respectively, for comparison with the original 321–323 K.

Fig. 9 presents the corresponding melting curves of paraffin with different melting temperatures. Paraffin with a low melting point melts sooner.

Fig. 10, Fig. 11 and Fig. 12 respectively correspond to the temperature curves of the bottom, middle, and top layers of paraffin wax with different melting temperatures. For the paraffin wax with a melting point of 311–313 K, the temperature at the bottom will rise greatly when it just reaches the melting point. Owing to the greater fluidity between the melted and liquid waxes, natural convection increases and heats up faster, and

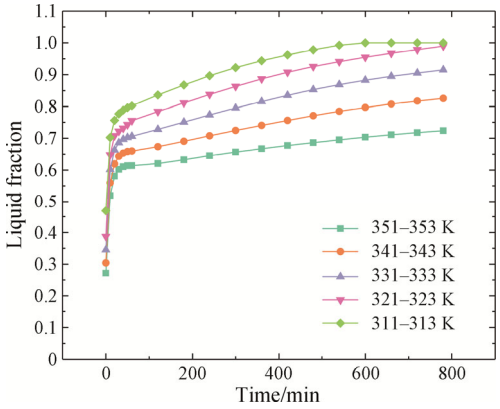

Fig. 9 The liquid fraction of paraffin with different melting temperatures

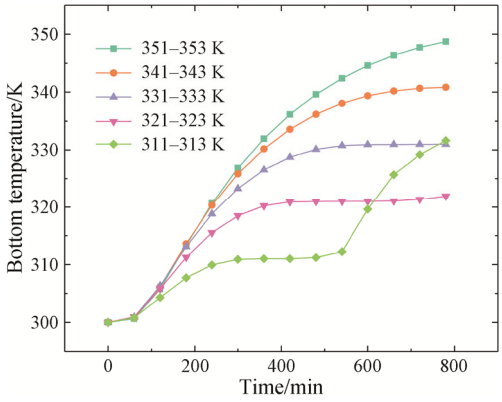

Fig. 10 Bottom temperature curves of paraffin with different melting temperatures

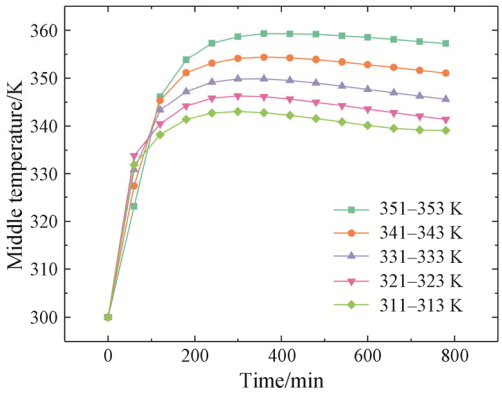

Fig. 11 Middle temperature curves of paraffin with different melting temperatures

there is a turning point on the line of 311–313 K. In a word, the higher the melting temperature of PCM is, the higher the overall temperature of the tank is. However, because there is less paraffin in the free state, the liquid fraction and temperature curve increase at a slower rate before reaching stability.

3.3 Effects of power of the electric heater

To explore the effects of different heating powers on the heat transfer characteristics of a paraffin-based single

tank, the total energy and the volume of the heating tube are guaranteed to be equal, but the heat power and heating time change. There are 5 different heating combinations. The power of the heater is 4000 W, 3500 W, 2500 W, and 2000 W; and the corresponding heating time is 540 s, 617 s, 864 s, and 1080 s, respectively, which are compared with 3000 W heating for 720 s in the original experiment.

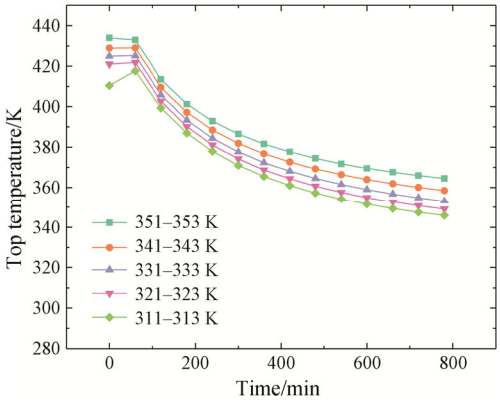

Fig. 12 Top temperature curves of paraffin with different melting temperatures

Fig. 13 shows the liquid fraction with different heating powers. Since the heating time is different, the initial heating time is taken as the zero point. When the total work is constant, the greater the heating power is, the faster the paraffin around the heater melts during heating process, and the faster the rate of natural convection in a short time. According to Fig. 14, when the heating power increases, the peak value of the top layer temperature is higher, but the power hardly affects the temperature curve before the peak value is reached, nor does it have much influence on the temperature curve after the inflection point. Therefore, the magnitude of power will only affect a small stage of the melting process, and will not have a great influence on the overall rate and results, which is almost negligible.

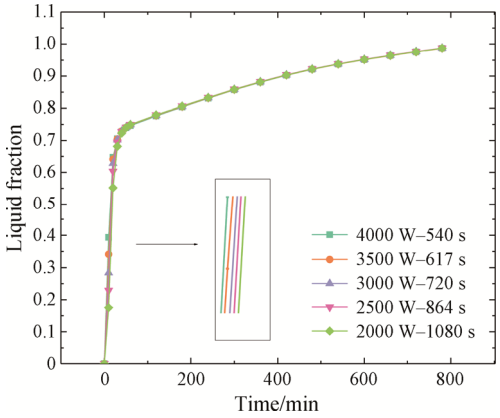

Fig. 13 The liquid fraction with different power of the heater

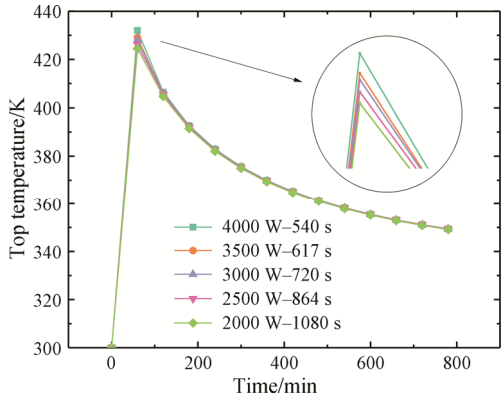

Fig. 14 Top temperature with different power of the heater

4. Conclusions

In this study, the paraffin-based solar single-tank heat storage platform was established, and the corresponding three-dimensional unsteady numerical model was established by FLUENT. The effects of the aspect ratio of the tank, the melting temperature of paraffin and the power of the electric heater on the melting process were studied numerically. The relevant conclusions are as follows:

(1) The numerical model established in this paper can successfully predict the heat transfer behavior of a single paraffin-based heat storage tank with a heating device.

(2) When maintaining a certain degree of paraffin filling, the closer the aspect ratio is to 1, the more uniform the natural convection-diffusion inside the tank is. The faster the heat diffuses, the shorter the melting time required for PCM. In this study, the liquid fraction went from 61.83% to 76.47% one hour after heating with the aspect ratio of the tank ranging from 2.8 to 1.1.

(3) When other thermal physical properties are constant, only the melting temperature of paraffin is changed. The higher the melting temperature of paraffin, the higher the overall temperature of the tank. However, it is more difficult for the PCM inside the tank to reach a stable state. Paraffin with the melting temperature of 311–313 K heats up faster at the bottom after melting.

(4) When the total power is guaranteed to be constant, changing the heating power and heating time has no great influence on the overall results, and the influence can be almost ignored in the design.

Acknowledgments

This work was supported by the National Natural Science Foundation of China (No. 51876147).

References

[1] Tauseef-ur-Rehman, Ali H.M., Janjua M.M., et al., A

critical review on heat transfer augmentation of phase change materials embedded with porous materials/foams. International Journal of Heat and Mass Transfer, 2019, 135: 649–673.

[2] Qureshi Z., Ali H.M., Khushnood S., Recent advances on thermal conductivity enhancement of phase change materials for energy storage system: A review. International Journal of Heat and Mass Transfer, 2018, 127: 838–856.

[3] Yuan Y., Ruan Z.H., Huang X., et al., Energy-absorption-based explanation of the TiO_2/C photocatalytic activity enhancement mechanism. Journal of Catalysis, 2017, 348: 246–255.

[4] Wang Z.Y., Diao Y.H., Zhao Y.H., et al., Experimental study on the new type of electrical storage heater based on flat micro-heat pipe arrays. Science China Technological Sciences, 2018, 61: 219–231.

[5] Zhang Y., Lu Y., Chen L., Energy harvesting via nonlinear energy sink for whole-spacecraft. Science China Technological Sciences, 2019, 62(9): 1483–1491.

[6] Mao Q., Recent developments in geometrical configurations of thermal energy storage for concentrating solar power plant. Renewable & Sustainable Energy Reviews, 2016, 59: 320–327.

[7] Wang F., Cheng Z., Tan J., et al., Progress in concentrated solar power technology with parabolic trough collector system: A comprehensive review. Renewable & Sustainable Energy Reviews, 2017, 79: 1314–1328.

[8] Chao X., Wang Z., He Y., et al., Parametric study and standby behavior of a packed-bed molten salt thermocline thermal storage system. Renewable Energy, 2012, 48: 1–9.

[9] Chao X.U., Xin L.I., Wang Z., et al., Effects of solid particle properties on the thermal performance of a packed-bed molten-salt thermocline thermal storage system. Applied Thermal Engineering, 2013, 57(1–2): 69–80.

[10] Xu C., Wang Z., He Y., et al., Sensitivity analysis of the numerical study on the thermal performance of a packed-bed molten salt thermocline thermal storage system. Applied Energy, 2012, 92: 65–75.

[11] Wu M., Xu C., He Y.L., Dynamic thermal performance analysis of a molten-salt packed-bed thermal energy storage system using PCM capsules. Applied Energy, 2014, 121(5): 184–195.

[12] Bellan S., Alam T.E., González-Aguilar J., et al., Numerical and experimental studies on heat transfer characteristics of thermal energy storage system packed with molten salt PCM capsules. Applied Thermal Engineering, 2015, 90: 970–979.

[13] Bellan S., Gonzalez-Aguilar J., Romero M., et al., Numerical analysis of charging and discharging performance of a thermal energy storage system with encapsulated phase change material. Applied Thermal Engineering, 2014, 71(1): 481–500.

[14] Bellan S., Matsubara K., Cho H.S., et al., A CFD-DEM study of hydrodynamics with heat transfer in a gas-solid fluidized bed reactor for solar thermal applications. International Journal of Heat and Mass Transfer, 2018, 116: 377–392.

[15] Kodama T., Bellan S., Gokon N., et al., Particle reactors for solar thermochemical processes. Solar Energy, 2017, 156: 113–132.

[16] Miguel S.Á.D., Bellan S., María J.M.G.D., et al., Numerical modelling of a 100-Wh lab-scale thermochemical heat storage system for concentrating solar power plants. American Institute of Physics Conference Series, 2016, 1734: 050005.

[17] Tay N.H.S., Bruno F., Belusko M., Experimental validation of a CFD model for tubes in a phase change thermal energy storage system. International Journal of Heat & Mass Transfer, 2012, 55(4): 574–585.

[18] Seddegh S., Wang X., Joybari M.M., et al., Investigation of the effect of geometric and operating parameters on thermal behavior of vertical shell-and-tube latent heat energy storage systems. Energy, 2017, 137: 69–82.

[19] Joybari M.M., Haghighat F., Seddegh S., Numerical investigation of a triplex tube heat exchanger with phase change material: Simultaneous charging and discharging. Energy & Buildings, 2017, 139: 426–438.

[20] Seddegh S., Joybari M.M., Wang X., et al., Experimental and numerical characterization of natural convection in a vertical shell-and-tube latent thermal energy storage system. Sustainable Cities and Society, 2017, 35: 13–24.

[21] Mao Q., Liu N., Peng L., et al., A novel shell-and-tube thermal energy storage tank: modeling and investigations of thermal performance. Applied Thermal Engineering, 2019, 159: 113964.

[22] Mao Q., Chen H., Zhao Y., et al., A novel heat transfer model of a phase change material using in solar power plant. Applied Thermal Engineering, 2018, 129: 557–563.

[23] Mao Q., Zhang L., Wu H., et al., Design and calculation of a new storage tank for concentrating solar power plant. Energy Conversion & Management, 2015, 100: 414–418.

[24] Joybari M.M., Haghighat F., Seddegh S., Natural convection characterization during melting of phase change materials: Development of a simplified front tracking method. Solar Energy, 2017, 158: 711–720.

[25] Chiu J.N.W., Martin V., Submerged finned heat exchanger latent heat storage design and its experimental verification. Applied Energy, 2012, 93(5): 507–516.

[26] Abdi A., Martin V., Chiu J.N., Numerical investigation of melting in a cavity with vertically oriented fins. Applied Energy, 2019, 235: 1027–1040.

[27] Chiu J.N., Martin V., Multistage latent heat cold thermal

energy storage design analysis. Applied Energy, 2013, 112: 1438–1445.

[28] Iranzo A., Suarez C., Guerra J., Mixing enhancement in thermal energy storage molten salt tanks. Energy Conversion and Management, 2018, 168: 320–328.

[29] Cheng X., Zhai X.Q., Wang R.Z., Thermal performance analysis of a packed bed cold storage unit using composite PCM capsules for high temperature solar cooling application. Applied Thermal Engineering, 2016, 100: 247–255.

[30] Fan L., Zhu Z., Xiao S., et al., An experimental and numerical investigation of constrained melting heat transfer of a phase change material in a circumferentially finned spherical capsule for thermal energy storage. Applied Thermal Engineering, 2016, 100: 1063–1075.

[31] Ming W., Chao X., He Y., Cyclic behaviors of the molten-salt packed-bed thermal storage system filled with cascaded phase change material capsules. Applied Thermal Engineering, 2016, 93: 1061–1073.

[32] Torregrosa-Jaime B., López-Navarro A., Corberán J.M., et al., Experimental analysis of a paraffin-based cold storage tank. International Journal of Refrigeration, 2013, 36(6): 1632–1640.

[33] Oró E., Gracia A.D., Castell A., et al., Review on phase change materials (PCMs) for cold thermal energy storage applications. Applied Energy, 2012, 99(6): 513–533.

[34] Mao Q., Li Y., Experimental and numerical investigation on enhancing heat transfer performance of a phase change thermal storage tank. Journal of Energy Storage, 2020, 31: 101725.

[35] Yang X.P., Yang X.X., Ding J., et al., Numerical simulation study on the heat transfer characteristics of the tube receiver of the solar thermal power tower. Applied Energy, 2012, 90(1): 142–147.

[36] Yang X., Yang X., Ding J., et al., Criteria for performance improvement of a molten salt thermocline storage system. Applied Thermal Engineering, 2012, 48(26): 24–31.

[37] Khalifa A.J.N., Hussian M.A., Heat flow in a horizontal solar thermal storage tank with an auxiliary heater. Energy Conversion and Management, 2002, 43(4): 549–555.

[38] Kibria M.A., Anisur M.R., Mahfuz M.H., et al., Numerical and experimental investigation of heat transfer in a shell and tube thermal energy storage system. International Communications in Heat & Mass Transfer, 2014, 53(4): 71–78.

[39] Barz T.J., Zauner C., Lager D., et al., Experimental analysis and numerical modeling of a shell and tube heat storage unit with phase change materials. Industrial & Engineering Chemistry Research, 2016, 55(29): 8154–8164.

[40] Q. Mao, Y. Li, M. Chen. Design and investigation of single tank phase change thermal storage domestic hot water system. Case Studies in Thermal Engineering, 2021, 25: 100903.